Enzyme Catalysis and Regulation:

Crystal Structure of Himalayan Mistletoe Ribosome-inactivating Protein Reveals the Presence of a Natural Inhibitor and a New Functionally Active Sugar-binding Site

Vandana Mishra, Sameeta Bilgrami, Radhey Shyam Sharma, Punit Kaur, Savita Yadav, Ruth Krauspenhaar, Christian Betzel, Wolfgang Voelter, Cherukuri R. Babu and Tej P. Singh

Access the most updated version of this article at doi: 10.1074/jbc.M500735200

Find articles, minireviews, Reflections and Classics on similar topics on the JBC Affinity Sites.

Alerts:

- When this article is cited
- When a correction for this article is posted

Click here to choose from all of JBC's e-mail alerts

This article cites 61 references, 11 of which can be accessed free at
http://www.jbc.org/content/280/21/20712.full.html#ref-list-1

Crystal Structure of Himalayan Mistletoe Ribosome-inactivating Protein Reveals the Presence of a Natural Inhibitor and a New Functionally Active Sugar-binding Site*

Vandana Mishra‡§¶‖, Sameeta Bilgrami‡, Radhey Shyam Sharma¶, Punit Kaur‡, Savita Yadav‡, Ruth Krauspenhaar**, Christian Betzel**, Wolfgang Voelter‡‡, Cherukuri R. Babu¶, and Tej P. Singh‡§§

*From the ‡Department of Biophysics, All India Institute of Medical Sciences, New Delhi 110 029, India, the §Department of Botany and the ¶Centre for Environmental Management of Degraded Ecosystems, School of Environmental Studies, University of Delhi, Delhi 100 007, India, the **Institute of Medical Biochemistry and Molecular Biology, 22603 Hamburg, Germany, and the ‡‡Institute of Physiological Chemistry, University of Tübingen, 72076 Tübingen, Germany*

Ribosome-inactivating proteins (RIPs) are toxins involved in plant defense. How the plant prevents autotoxicity is not yet fully understood. The present study is the first structural evidence of a naturally inhibited form of RIP from a plant. Himalayan mistletoe RIP (HmRIP) was purified from *Viscum album* leaves and crystallized with lactose. The structure was determined by the molecular replacement method and refined at 2.8-Å resolution. The crystal structure revealed the presence of high quality non-protein electron density at the active site, into which a pteridine derivative (2-amino 4-isopropyl 6-carboxyl pteridine) was modeled. The carboxyl group of the ligand binds strongly with the key active site residue Arg[162], nullifies the positive charge required for catalysis, and thereby acts as a natural inhibitor. Lectin subunits of RIPs have two active sugar-binding sites present in 1α- and 2γ-subdomains. A third functionally active site has been identified in the 1β-subdomain of HmRIP. The 1β-site is active despite the absence of conserved polar sugar-binding residues. Loss of these residues is compensated by the following: (i) the presence of an extended site where the penultimate sugar also interacts with the protein; (ii) the interactions of galactose with the protein main chain carbonyl and amide nitrogen atoms; (iii) the presence of a well defined pocket encircled by four walls; and (iv) a favorable stacking of the galactose ring with Tyr[66] besides the conserved Phe[75]. The mode of sugar binding is also distinct at the 1α and 2γ sugar-binding sites.

Ribosome-inactivating proteins (RIPs)[1] are translation inhibitors, mainly present in plants (1). They act as defense proteins in plants (2, 3). Recent studies suggest that they can directly inhibit the plant pathogens by inactivating their ribosomes, causing cell death (4). RIPs inhibit translation by their *N*-glycosidase activity. They remove a specific adenine (4324) from the universally conserved GAGA hairpin loop in 28 S rRNA. This abolishes the ability of rRNA to bind to the elongation factor and, thus, inhibits protein synthesis (5). RIPs not only release adenine from the rRNA but also DNA as well as poly(A) under *in vitro* conditions (6, 7). Based on the number and nature of subunits, RIPs are broadly classified into the following two types: (i) type I, monomeric glycoproteins with a molecular mass of ~30 kDa; and (ii) type II, heterodimeric proteins having an enzymatic and a lectin subunit of ~30 kDa each. Type III RIPs are the newly discovered monomeric proteins (<30 kDa) present in the inactive form in the cytoplasm that get activated upon removal of a catalytic peptide (8). RIPs are pharmacologically important proteins (9), having potential applications in the treatment of deadly diseases in humans such as cancer and AIDS (10, 11). Immunotoxins have been synthesized by linking RIPs with the antibodies developed against a surface constituent of the tumor cells. The immunotoxins specifically recognize and kill the tumor cells by inhibiting their protein synthesis and show promising results both *in vitro* and *in vivo*.

The autologous toxicity of RIPs on the plant ribosomes under *in vitro* conditions has been demonstrated by several workers, but how the plants prevent the autotoxicity *in vivo* is not yet fully understood (12, 13). It seems that plants have evolved some cellular protective mechanisms to ensure their survival. Compartmentalization of the toxin into specific cell organelles is one of the proposed strategies (14). The presence of cellular inhibitors is another possibility. Many hydrolytic enzymes stored in plant vacuoles are known to be present in naturally inhibited form (15). The enzyme inhibitor complex gets dissociated when required, and the degradation of the substrate is initiated. Several investigators have proposed the presence of natural inhibitors for RIPs also (16). The natural inhibitor of a type I RIP from *Phytolacca americana*, PAP, has been purified and characterized (17, 18). However, no such natural inhibitor for the type II RIPs has yet been identified.

The mistletoe RIPs are of type II family derived from the hemi-parasitic plant *Viscum album*. They constitute the active principle of the anti-tumor mistletoe preparations widely used in Europe (19, 20). Interestingly the antitumor effect appears to be the result of their immunomodulatory properties rather than toxicity (21, 22). The clinical studies have shown that the lectin subunit of ML-I enhances the secretion of cytokines and interleukins and increases the number of natural killer cells. Because recognition and binding to the sugar chains present on the cell surface of immunogenic cells are proposed as being the first step in the biological activity (23), the variations in the sugar binding properties of the RIPs have significance in determining their medicinal potential. The lectin moiety not only recognizes the glycoproteins and glycolipids present on the cell surface but also binds to the intracellular galactose receptors and facilitates the routing of toxin within the cells (24). Consequently, unveiling the mode of sugar binding has immense potential in understanding the mechanism of action of RIPs. The Himalayan mistletoe ribosome inactivating protein (HmRIP) has been purified from *Viscum album*, inhabiting the northwestern Himalayas (25). It is known for its unique sugar binding properties. In the present study, the natural complex formed between HmRIP and its inhibitor (2-amino 4-isopropyl 6-carboxyl pteridine) was crystallized with lactose, and the structure was determined at 2.8-Å resolution.

EXPERIMENTAL PROCEDURES

Plant Material and Purification of HmRIP in Its Natural Form— Field surveys of the northwestern Himalayas were carried out for the collection of plant material. The Gouraghati reserve forest, at a height of >6000 feet in the Chakrata ranges of the Himalayas was selected as the sampling site. Himalayan mistletoe (*V. album*), the hemi-parasitic plant parasitizing the wild apple (*Pyrus pashia*), was collected along with the host stem and brought to the lab and stored at −20 °C.

The frozen leaf tissues were crushed into fine powder in presence of liquid nitrogen. The total soluble protein was extracted in 0.2 M sodium acetate buffer containing 0.5 M NaCl (pH 3.5). Crude extract was filtered through a muslin cloth and centrifuged at 12 000 × g for 30 min. The supernatant was filtered through 0.2-μ filter. An affinity chromatography column was packed with partially hydrolyzed Sepharose 4B (25) and equilibrated with sodium acetate buffer containing 0.5 M NaCl (pH 3.5). The sterile filtered crude extract was loaded on the affinity column. The unbound proteins were washed off with the same buffer. The bound protein was eluted as a single peak with 0.2 M lactose in the same buffer. All of the fractions forming the peak were pooled and concentrated by ultrafiltration.

Crystallization of HmRIP-I with Lactose—A concentrated sample of the HmRIP and lactose complex (0.1 M) was prepared in 0.1 M glycine-HCl buffer (pH 3.5). The reservoir solution contained 0.1 M glycine-HCl (pH 3.5), 25% $(NH_4)_2SO_4$ and 0.2 mM NaCl. The 10-μl drops of protein solution were made and placed on the cover slips for the hanging drop vapor diffusion method against the reservoir solution of 1000 μl in a vial. After 3 weeks, hexagonal bipyramidal crystals were obtained at 298 K.

X-ray Intensity Data Collection and Processing—The x-ray intensity data were collected using synchrotron beam line X13 operated by the European Molecular Biology Laboratory outstation at Deutsches Elektronen Synchrotron, Hamburg, Germany on a MAR image plate scanner. The crystals were flash-frozen to 100 K. Using a wavelength of λ = 0.8459-Å resolution, the data were processed with DENZO and SCALE-PACK programs (26). The crystals belong to hexagonal space group P6 (5)22 with $a = b = 109.4$ Å and $c = 309.8$ Å. The details of data collection and processing are listed in Table I.

Structure Solution and Refinement—The structure was determined with the molecular replacement method using AMoRe (27). The coordinates of the native HmRIP structure were used as the starting model (28). A distinct solution was obtained for a single heterodimer (having the enzyme, an A chain and lectin, a B chain), which gave a correlation coefficient and R-factor of 58.7 and 42.2%, respectively, after rigid body refinement. The model was refined using REFMAC (29). Because, the solvent content of the crystals of HmRIP was high (73%), TLS refinement was carried out (30). Two rigid bodies were defined as chains A and B, and their movements were modeled. This improved the quality of electron density. Both of the chains were manually adjusted sepa-

TABLE I
Crystallographic data and refinement statistics

Data collection statistics	
Protein data bank code	1YF8
Space group	P6$_5$22
Unit cell dimensions (Å)	
$a = b$	109.4
c	309.8
V_m (Å^3/Da)	4.7
Solvent content (%)	73.8
Resolution range (Å)	20.0–2.8
Number of unique reflections	26,570
Completeness^a (%)	95.8 (99.7)
R_{sym}^{a} (%)	5.7 (33.6)
Overall^a $I/\sigma I$	11.0 (2.0)

Refinement statistics	
R_{cryst} (%)	23.4
R_{free} (%)	28.7
Protein atoms	4018
Lactose (atoms)	2 (46)
Galactose (atoms)	1 (11)
Mannose (atoms)	3 (33)
N-acetyl glucosamine (atoms)	7 (98)
AICP (atoms)	1 (17)
Water molecules	107
R.m.s.^{b} deviation in bond lengths (Å)	0.01
R.m.s.^{b} deviation in bond angles (°)	2.2
Average *B*-factor from Wilson plot (Å^2)	91.1
Average *B*-factor for all atoms (Å^2)	91.8
Residues in the most allowed regions (%)	81.3
Residues in the additionally allowed regions (%)	18.7

^{a} Last shell (2.85–2.8) values given in parentheses.
^{b} Root mean square.

rately using program O (31) into the improved density with intermittent cycles of refinement with REFMAC. This gave an *R*-factor of 0.32. The model was rebuilt extensively using maps calculated at this stage. This map also showed good electron densities for carbohydrate moieties at Asn^{107} in chain A and Asn^{57}, Asn^{92}, and Asn^{132} in chain B, galactose and lactose molecules at sugar-binding sites in chain B, and a ligand at the active site in chain A. The electron densities clearly allowed the interpretation of one *N*-acetyl glucosamine molecule at Asn^{107} in chain A (Fig. 1*A*, *NAG1*), two *N*-acetyl glucosamine residues and one mannose residue at Asn^{57} (Fig. 1*B*, *NAG1*, *NAG2*, and *MAN3*), two *N*-acetyl glucosamine residues at Asn^{92} (Fig. 1*C*, *NAG1* and *NAG2*), and two *N*-acetyl glucosamine and two mannose residues at Asn^{132} (Fig. 1*D*, *NAG1*, *NAG2*, *MAN3*, and *MAN4*) in chain B. The good electron density also allowed us to model one galactose molecule at the 1α sugar binding site (Fig. 2*A*), and one lactose molecule each at the 1β (Fig. 2*B*) and 2γ (Fig. 2*C*) sugar-binding sites. For the first time a sugar molecule has been identified at the 1β sugar-binding site. Yet another non-protein density was clearly interpreted as the 2-amino 4-isopropyl 6-carboxyl pteridine (AICP) molecule, presumably as a potent inhibitor of HmRIP (Fig. 3). 107 water molecules were also included in the model provided they met the criteria of peaks >3 σ in $|F_o - F_c|$ maps and hydrogen bond partners with appropriate distance and angle geometry. All of these residues/molecules were included in the further cycles of refinement and manual model building. The model was improved by calculating a series of omit maps at each stage of refinement. The final *R* and R_{free} factors were 0.234 and 0.287, respectively. A Ramachandran plot of the main chain torsion angles (ϕ, ψ) shows that 81.3% of the residues are in the most favored regions as defined in the program PROCHEK (32, 33). The refinement statistics are given in Table I.

RESULTS AND DISCUSSION

The Overall Structure—The general organization of HmRIP (Fig. 4) is essentially similar to that observed for other type II RIPs (34–39). It is a heterodimer containing a chain A with *N*-glycosidase activity and a chain B with lectin activity. On the other hand, a closely related member of the family ML-I can exist as a heterodimer as well as a tetramer consisting of two heterodimers.

The chain A is divided into two non-homologous domains (Fig. 4), A1 (1–13, 44–155) and A2 (14–43, 156–239). A significant deletion after Ser^{88} in the domain A1 results in the loss of
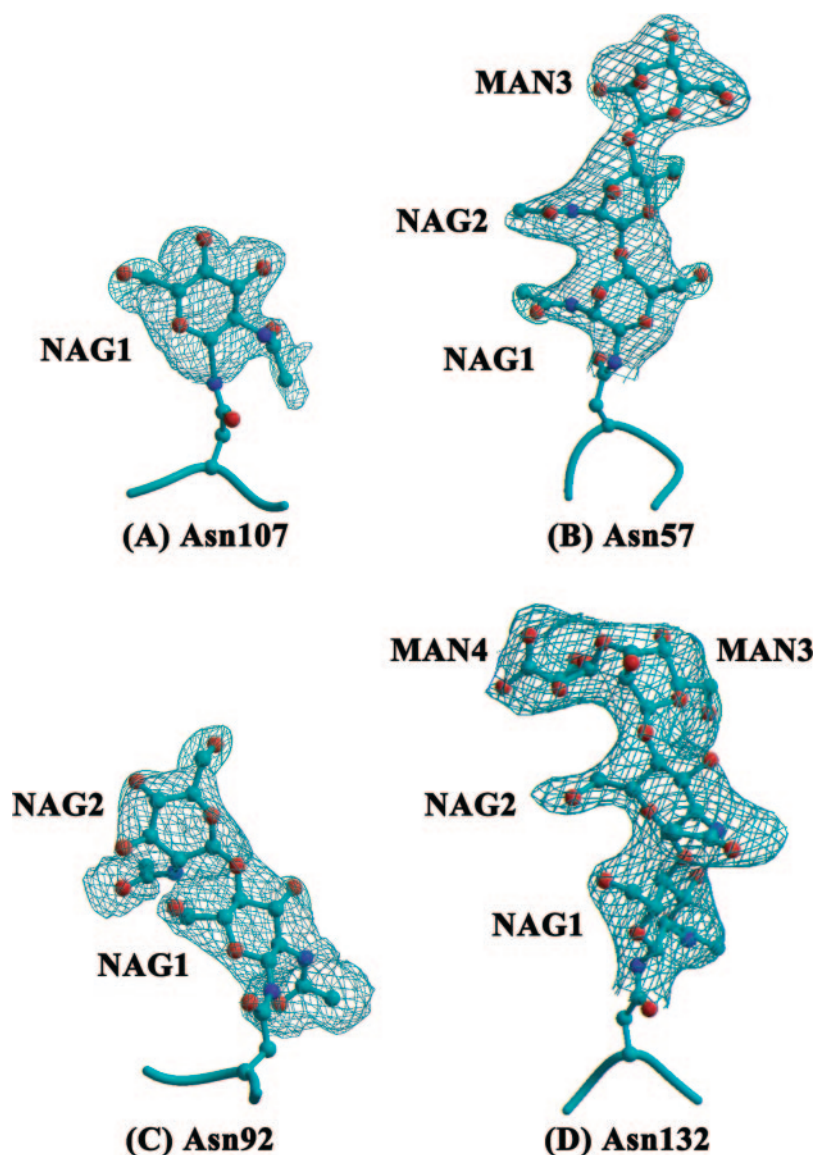
FIG. 1. |$2F_o - F_c$| **electron density map of the sugar chains present at the glycosylation sites at Asn[107] (A) in chain A and Asn[57] (B), Asn[92] (C), and Asn[132] (D) in chain B of the HmRIP.** The figure was prepared in Bobscript (62). *MAN*, mannose; *NAG*, *N*-acetyl glucosamine,

one complete helix. This domain is comprised of one mixed β-sheet and three α-helices, α2, α3, and α4 (28), in contrast to the four helices observed in ML-I, ricin, abrin, ebulin, trichosanthin, etc. The helix α4 crosses over from the A1 to the A2 domain. The A2 domain contains four α-helices, α1 and α5–α7, and four β-strands, β2-β3, β9, and β10. The *N*-glycosidase activity site is situated in the cleft formed by the association of domains A1 and A2 (Fig. 4). Tyr[75], Tyr[110], Glu[159], Arg[162], and Trp[193] are the key residues involved in substrate binding and catalytic activity. In the A1 domain of the HmRIP, a 22-Å-wide cavity has been identified as the ribosome recognition site (28). The conserved β-strands β5 and β6 form the base of the cleft, whereas the loops between β3 and β4, β8 and α2, and β7 and β8 form the walls. Four conserved residues, Arg[51], Asp[70], Thr[72], and Asn[73], represent the binding residues. The ribosome recognition site is a shallow cleft present on the surface, whereas the *N*-glycosidase activity site corresponds to a well defined deep pocket. Both sites are clearly connected through a shallow channel. The distinct demarcation between the ribosome recognition site and the *N*-glycosidase activity site and the gigantic size of substrates such as the ribosome suggest a double step mechanism of action. In this mechanism the ribosome binds to the ribosome recognition site first, which holds it in a favorable way for the attack against the rRNA in the second step.

The basic structure of chain B is highly conserved among the type II RIPs (34–38). It folds into two well separated homologous domains, B1 (1–132) and B2 (133–255). Each of these two domains is mainly comprised of three subdomains *i.e.* α, β, and γ (Fig. 4). The α- and β-subdomains are represented by a pair of anti-parallel β-sheets joined by a loop. The γ-subdomains are truncated and lack the C-terminal strand from the second β-sheet. All of the subdomains except the 1α and 1γ contain a 3_{10} helix in between the two β sheets. λ-Subdomains, which are unrelated to the α-, β-, and γ-subdomains, also constitute part of chain B. The 1λ-subdomain connects chain A with chain B and the 2λ-subdomain links the domain B1 with domain B2. Subdomains 1β, 2α, and 2β contain an S–S bond between the conserved Cys residues. On the other hand, the substitutions of Asn[17] and Ser[36] for Cys residues in the 1α-subdomain rule out the formation of the standard disulfide bond. The homologous disulfide bridge is also absent in ML-I, although it is conserved in ricin, abrin, and ebulin. The lack of an S–S bond and involvement of the amino acid residues Tyr[64], Ala[68], Gly[69], Val[70], Arg[21], Asp[22], Gly[28], Gln[30], Ser[107], Ile[110], Thr[114], and Gln[118] were proposed to be responsible for the tetramerization of ML-I (34). Despite all these features, HmRIP remains in the heterodimeric form.

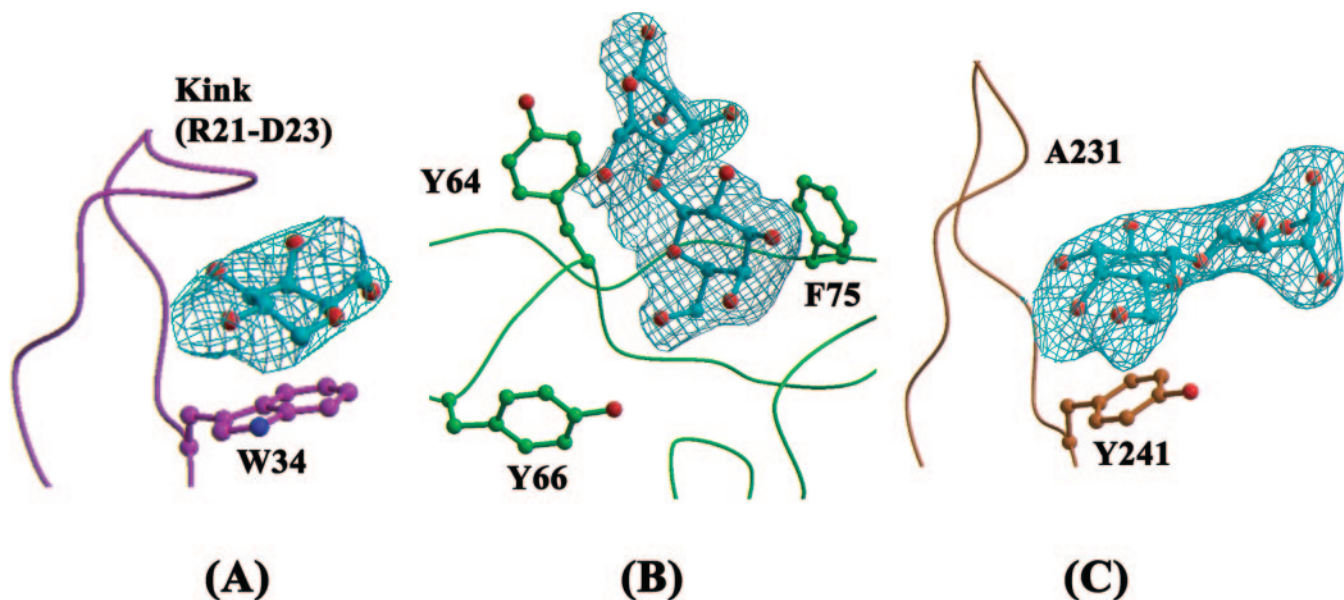The chains A and B of HmRIP are associated mainly by

FIG. 2. **The $|F_o - F_c|$ electron density map for the sugar molecules contoured at 3 σ.** *A*, at the 1α sugar-binding site galactose sits nicely between the two walls formed by the conserved aromatic residue Trp[34] (*W34*) and the kink, Arg[21]-Asp[23] (*R21-D23*), in the main chain. *B*, lactose is bound at the 1β sugar-binding site, Tyr[64]-Tyr[66] (*Y64* and *Y66*) form the kink, and Phe[75] (*F75*) is the conserved aromatic residue. *C*, at the 2γ sugar-binding site the kink is absent and the region is represented by Ala[231] (*A231*); lactose is oriented parallel to the aromatic ring of Tyr[241] (*Y241*).
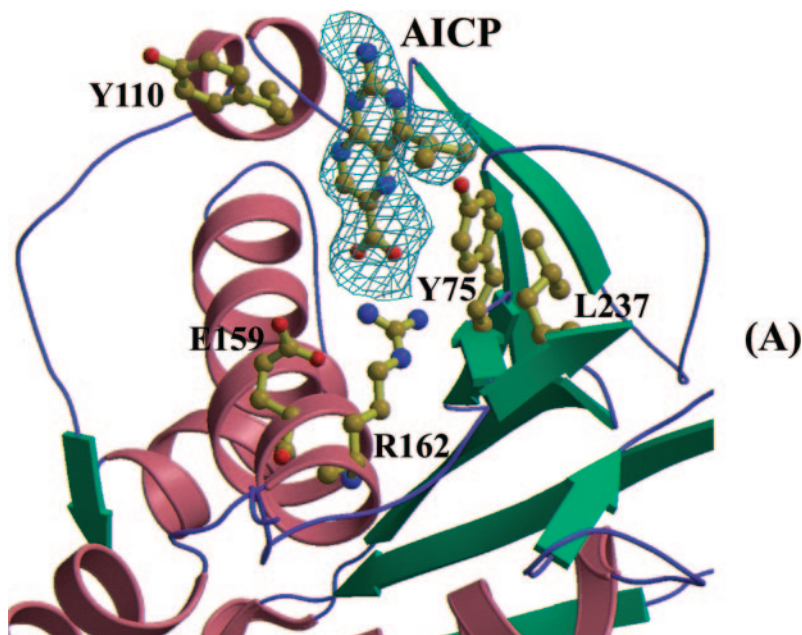
FIG. 3. *A*, *N*-glycosidase activity site showing the $|F_o - F_c|$ electron density map for AICP contoured at 3 σ. The key active site residues are shown in *ball-and-stick* model. Single letter amino acid abbreviations are used with position numbers here. *B*, chemical drawing of the AICP showing the atom numbering.

hydrophobic and a few polar interactions. The H-bond between Glu[205] (A) Oϵ2 and Arg[50] (B) NH1 is one of the specific interactions joining A and B subunits of HmRIP. Because of the substitution of Glu[205] by Asp in ML-I, the homologous interaction is absent.

HmRIP in Its Naturally Inhibited Form—The HmRIP is

Crystal Structure of HmRIP-Natural Inhibitor Complex

FIG. 4. **Ribbon diagram of the HmRIP structure (heterodimer) showing the A chain (enzyme) and B chain (lectin).** The newly identified natural inhibitor AICP is bound at the *N*-glycosidase active site between the A1 and A2 domains. In the B1 domain, galactose is bound at the 1α-subdomain (*pink*), and lactose is bound at the 1β-subdomain (*green*). In the B2 domain, lactose is bound at the 2γ-subdomain (*mustard*). Sugar chains at the glycosylation sites are shown in *gray*. The figure was prepared using MolScript (63) and Raster3D (64). Single letter amino acid abbreviations are used with position numbers here.
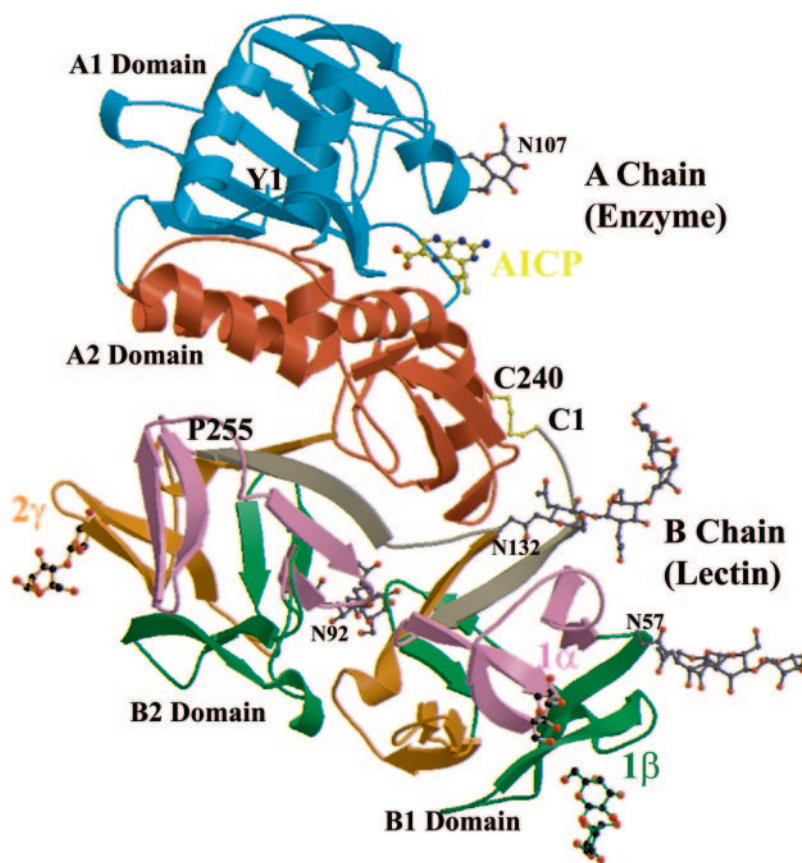
localized inside the plant vacuole (40), which has an acidic environment. In the present study, HmRIP was purified and crystallized under acidic conditions (pH 3.5). The present crystal structure represents the model of HmRIP under acidic conditions. It was remarkable to observe an excellent quality of non-protein electron density at the active site (Fig. 3). The density was highly characteristic, into which an AICP molecule was modeled nicely. It showed clear contacts with the key active site residue, Arg162, even at the 2.5 σ cutoff in the $|2F_o - F_c|$ map. Synthetic pteridine derivatives have been identified as some of the most potent inhibitors of RIPs *in vitro* (41–43). Some of the pteridine derivatives are also abundant in plant vacuoles and are known to inhibit the enzymes involved in the purine metabolism (44). Based on these data and the highly characteristic electron density, it was clear that a derivative of pteridine was the most compatible molecule at the active site. The side groups were added to the pteridine ring structure, taking clues from the electron density and the negative-positive electrostatic regions of the active site. The AICP molecule matched perfectly in the active site and interacted effectively. AICP molecule adopts an excellent orientation and operates like a specific lid blocking the gate of the active site of HmRIP. The side chain of Tyr[110] was found flipped outside in the most contrasting manner and provides sufficient space to the inhibitor. The AICP ligand forms several interactions with a number of key residues at the *N*-glycosidase active site of the toxin subunit (Fig. 5A). The most significant interactions are formed between the carboxyl group of the inhibitor and the guanidium group of Arg[162]. Tyr[75] OH also interacts with the N5 atom of the ligand. It may be mentioned that the Arg[162] and Tyr[75] have been identified as the most critical residues for the *N*-glycosidase activity of RIPs (45). Tyr[110] N and Ser[109] Oγ interact with the AICP atoms N8 and N1, respectively. In addition to the hydrogen bonds, the propyl group of the inhibitor forms hydrophobic interactions with Leu[237]. This is in direct contrast with

most of the synthetic inhibitors, which rely mainly on the bonds formed with the main chain carbonyl and amide nitrogen atoms of Gly[108] and Val[76], which belong to the β8-α2 loop and the β6 strand, respectively. They may also have a weak N–N bond with the key catalytic Arg. The pteroic acid based inhibitors of ricin and ebulin make only a few contacts with Arg[162].

Several mechanisms have been proposed for *N*-glycosidase activity of RIPs (39, 46, 47). Except for one (48), all of the mechanisms commonly highlight the essentiality of the positive charge at Arg[162] for catalysis. The importance of the positive charge was also confirmed by site-directed mutagenesis (49). It is very clear from the interactions that the AICP molecule specifically and strongly binds with the active site Arg[162]. The carboxyl group of the AICP nullifies the positive charge on the Arg[162], which is essential for catalysis and thereby inhibits the activity of HmRIP. In contrast, synthetic inhibitors of ricin and ebulin are deeply embedded inside the cleft, mimicking the adenine base and other substrate analogs (Fig. 5B) (42, 50, 51). They inhibit by occupying all of the space in the active site cleft. Their deep seated location, orientation, and strong nonspecific bonding make their dissociation and reactivation difficult. On the other hand, the strong and specific interactions of AICP with important catalytic residues indicate that it acts as an inhibitor. Its appropriate orientation and shallow placement suggests that it will be able to easily dissociate when required.

Functionally Active Sugar-binding Sites of HmRIP—Lectin subunits of RIPs have evolved by gene triplication and then duplication of a primitive 40-residue galactose binding peptide, giving rise to the six subdomains (52). Each subdomain is made up of two antiparallel β-sheets, βI and βII, connected by a 3₁₀-helix or a coil (βI-βII segment). The sugar-binding site is constituted by the two-stranded βI sheet and the βI-βII segment. An aromatic ring on the one side and a three-residue kink on the other side form the two "walls" of the sugar-binding site. The essential aromatic residue comes from the C terminus
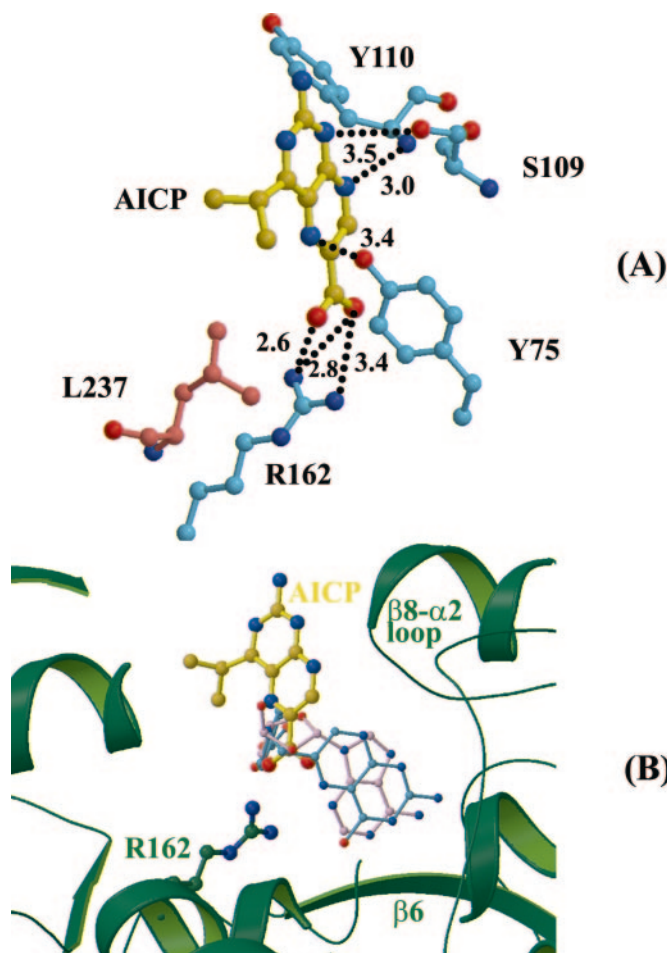
(A)

(B)

FIG. 5. *A*, interactions between the AICP (*yellow*) and the residues of the *N*-glycosidase activity site of chain A, which is divided between the A1 domain (*cyan*) and the A2 domain (*Indian red*). Carboxyl group of inhibitor forms H-bonds with the guanidium group of Arg[162]. The isopropyl group of the inhibitor forms van der Waals interactions with Leu[237] of HmRIP. *B*, differences in the placement of the natural inhibitor AICP (*yellow*), the synthetic inhibitor of ricin, pteroic acid (*cyan*), and the substrate analog adenine (*pink*), showing the deep seated orientation of synthetic inhibitor between the β6 strand and the β8-α2 loop. AICP with shallow placement has a strikingly different orientation. Single letter amino acid abbreviations are used with position numbers here.

of the second β-strand of the βI sheet and forms stacking interactions with the sugar. The kink is formed from the C terminus of the first β-strand. The residues from N terminus of first β-strand and the βI-βII segment provide polar interactions to the sugar. Structural studies on RIPs revealed that of the six possible galactose binding subdomains, only two subdomains, 1α and 2γ, satisfy the three structural criteria proposed to be essential for the sugar binding, *i.e.* a conserved aromatic residue, a three-residue kink, and conserved polar residues (Asp and Asn), and, therefore, retain the functional activity (53). The absence of any one of the above mentioned features has been proposed to result in the loss of sugar binding ability of the 1β, 1γ, 2α, and 2β subdomains.

Detection of A New, Functionally Active Sugar-binding Site in 1β-Subdomain—We have identified the presence of a third functionally active sugar-binding site in the 1β-subdomain of HmRIP. In the 1β-site, Phe[75] represents the aromatic residue and Tyr[64]-Tyr[66] forms the kink. The domain was thought to be functionally inactive due to the absence of the conserved sugar-binding residues (53). The residue corresponding to the conserved Asp is replaced by Thr[62], and Asn is mutated to Ala[84]. Despite these changes, exceptionally clear electron density was
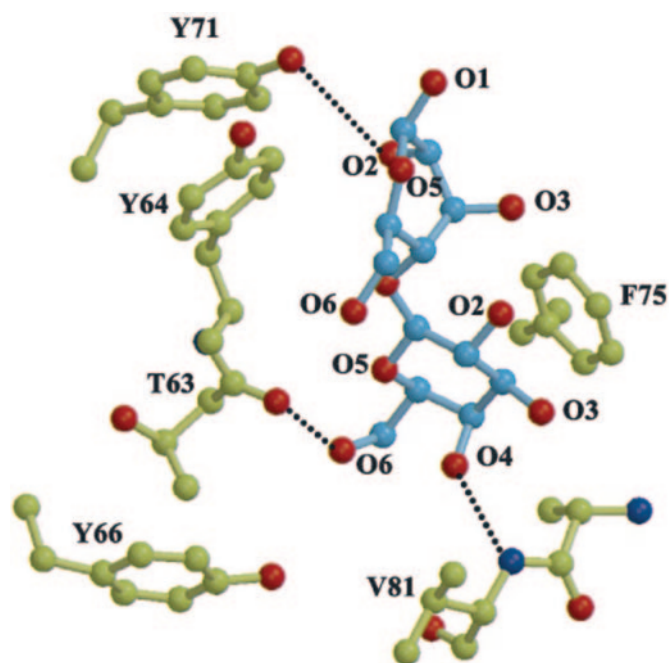

FIG. 6. **Interactions between lactose (*cyan*) and sugar-binding residues (*green*) at the 1β-site of HmRIP.** Galactose makes stacking interactions with the aromatic ring of Phe[75] (*F75*) and Tyr[66] (*Y66*) and sugar O6 and O4 interact with the main chain carbonyl oxygen of Thr[63] (*T63*) and the amide nitrogen of Val[81] (*V81*), respectively. Glucose stacks with the aromatic ring of Tyr[64] (Y64), and the O2 of glucose also makes an H-bond with Tyr[71] OH.

observed for the complete lactose molecule (Fig. 2*B*). The apolar face of the galactose stacks favorably with the aromatic ring of the Phe[75]. In addition, the O6 of the sugar interacts with the main chain carbonyl oxygen of Thr[63] adjacent to the kink region (Fig. 6). The O4 of the sugar interacts with the main chain nitrogen of Val[81], coming from the βI-βII segment. Furthermore, Tyr[66] orients in a way that it is almost parallel to the side chain ring of the Phe[75], stacking the sugar between two aromatic residues. Interestingly, the glucose of the lactose also interacts extensively with the protein. Tyr[64] stacks with the glucose ring. The O2 of the glucose also interacts with the OH of another conserved Tyr[71].

A detailed analysis of the architecture and mode of lactose binding at the 1β-site reveals the reasons for the site being active. The conformation of the βI-βII segment is very different at the 1β-site. As compared with the 1α- and the 2γ-sites, it is situated much closer to the three-residue kink and aligns parallel to it (Fig. 7*A*). Tyr[66] also stacks with the Phe[75], making a well defined pocket bound by four walls, *i.e.* the kink, Phe[75], Tyr[66], and the βI-βII segment. In contrast, the 1α and 2γ sugar-binding sites are lined by only two walls.

A number of lectins recognize an additional sugar moiety apart from the primary determinant even though they do not show any significant activity for the second sugar as a monosaccharide. Such sites have been defined as extended sugar-binding sites (54). The plant lectins use the extended site as an additional feature to enhance their sugar binding ability. The extensive interactions of the glucose ring with Tyr[64] and Tyr[71] in HmRIP (Fig. 6) suggest that the 1β-subdomain has an extended sugar-binding site that enhances its ability to bind sugars and compensates, in part, for the loss of the polar sugar-binding residues. The presence of an extended site has not been indicated in any RIP by structural studies.

The sugar binding studies carried out on ML-I and ricin proposed it to have an extended sugar-binding site (55–57).
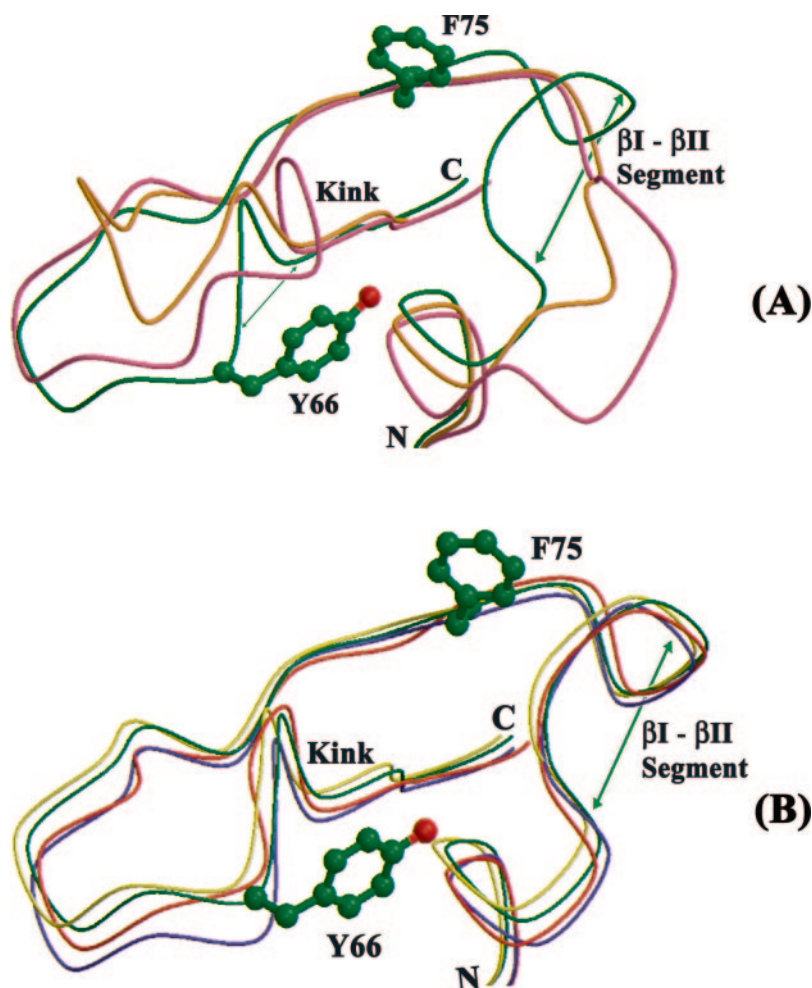
FIG. 7. *A*, superposition of the 1α (*pink*), 1β (*green*), and 2γ (*mustard*) sugar-binding sites of HmRIP, showing their different conformations. At the 1β-site the βI-βII segment has moved toward the kink, such that the sugar binding pocket is a well defined shallow cavity lined by the four walls consisting of the kink, the βI-βII segment, and the side chain of Phe[75] (*F75*) and Tyr[66] (*Y66*). *B*, superposition of the 1β-site of HmRIP (*green*) with ML-I (*yellow*), ricin (*blue*), and ebulin (*red*), showing architecture similar to that of the sugar binding pocket.

However, the crystal structures of the lactose complexes with RIPs disclosed only two functionally active sugar-binding sites, each of which did not have any extended sugar binding site (34, 36). A comparative analysis of the structures of 1β-site in HmRIP, ML-I, and ricin revealed that the overall architecture of the site is similar in all of them (Fig. 7*B*). The conformation of the βI-βII segment forming the third wall is conserved. The aromatic residues Phe[75] and Tyr[66] that form stacking interactions with the galactose are present and adopt similar conformations. The other aromatic residue, Tyr[64], which stacks with the pyranose ring of the penultimate sugar (glucose of lactose), is also conserved. The above observations provide evidence for the functional studies carried out on ML-I and ricin (55–57) and suggest that the 1β-site may be active in ML-I and ricin. The overall architecture of the 1β-site of ebulin is also similar to that of HmRIP, ML-I, and ricin (Fig. 7*B*); however, the key sugar-binding residues of the 1β-site, Phe[75], Tyr[64], and Tyr[66], are mutated to Thr, Asn, and Leu, respectively. The absence of key sugar-binding residues of the 1β-site in ebulin points toward the possibility of its being inactive.

Conserved 1α Sugar-binding Site—In the 1α-site, all of the features proposed as being essential for sugar binding are conserved, and the overall architecture of the site in HmRIP is essentially similar to that of other RIPs. The Arg[21]-Asp[23] comprises the kink region, and Trp[34] represents the conserved aromatic residue. The conserved polar residues involved in sugar binding are Asp[19] and Asn[43]. Their conformations are also similar to those found in the other RIPs. The electron density was present only for the galactose moiety at this site (Fig. 2*A*). The galactose occupies the space between the two

walls formed by Trp[34] and the kink. Despite the highly conserved architecture of the site, the galactose adopts an entirely different conformation in the HmRIP. The pyranose ring of the sugar is rotated at an angle of ~90° with respect to the galactose bound in ML-I, ricin, and ebulin (Fig. 8*A*). The galactose is shifted slightly toward the Trp[34] in a way that the non-polar face makes very strong stacking interactions with the Trp ring, so much so that the electron density of the sugar is continuous with that of the Trp ring even at the 2 σ cutoff in a $|2F_o - F_c|$ map. The Asp19 Oδ1 and Oδ2 form strong H-bonds with galactose O3 and O2 in HmRIP (Fig. 8*B*), whereas the homologous Asp interacts with O3 and O4 in ML-I, ricin, and ebulin. The Asn[43] Nδ2 interacts with O3 in HmRIP. The interaction between the corresponding Asn and galactose O3 is conserved in all the RIPs. Gln[32] Nε2 interacts with the O3 in HmRIP, O4 in ML-I, O4 and O6 in ricin, and O6 in ebulin. The main chain amide nitrogen atom of Asp[22] belonging to kink region makes an H-bond with galactose O3 and O4. The respective nitrogen interacts with O4 in ML-I and ebulin and O4 and O6 in ricin. Nζ of Lys[37], which comes from the βI-βII segment, makes strong H-bonds with galactose O2 in HmRIP and O2 and O3 in ricin and ML-I. The Lys[37] also makes important interactions with Asn[43] and stabilizes the conformation of this key sugar-binding residue. The corresponding Lys is mutated to Gly in ebulin (37). In addition, the deletion of two residues shortens the βI-βII segment in ebulin. This allows the side chain of Gln[44] (numbering as in ebulin) coming from the other side of the βI-βII segment to take the space occupied by the Lys in the other RIP structures and makes similar interactions. Gln[44] Oε1 interacts with the O3 of sugar and also interacts with the Nδ2
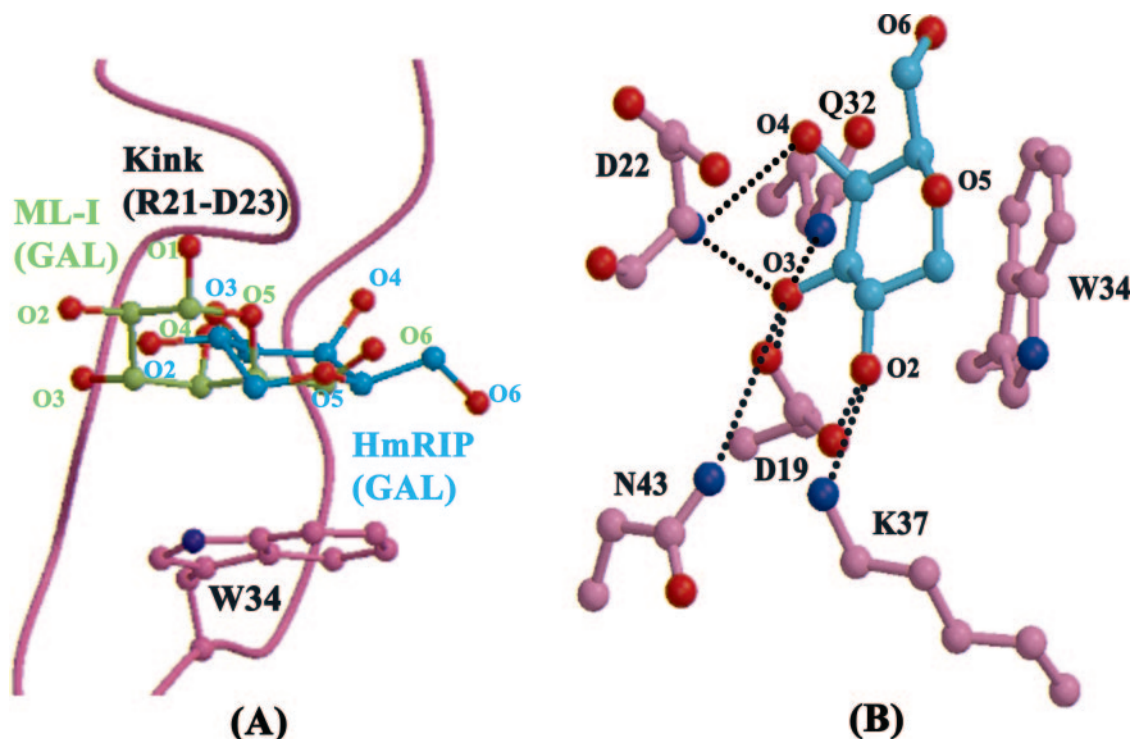
FIG. 8. *A*, superposition of the galactose bound (*GAL*) at the 1α sugar-binding site of HmRIP (*cyan*) and ML-I (*green*). The pyranose ring of galactose is oriented at an angle of 90° in HmRIP in comparison with ML-I. *B*, interactions between galactose (*cyan*) and sugar-binding residues (*pink*) at the 1α-site of HmRIP. Galactose makes stacking interactions with the aromatic ring of Trp[34] (*W34*). H-bonds are mainly formed by the O2 and the O3 of galactose. Single letter amino acid abbreviations are used with position numbers here.

of conserved Asn and stabilizes it. Thus, this position seems to be important in the 1α-site.

2γ Sugar-binding Site with a Distinct Conformation—The overall architecture of the 2γ-site in HmRIP is significantly different from that observed in ML-I, ricin, and ebulin. Because of the deletion of two critical residues after Ala[231], the kink is completely absent in the 2γ-site (26, 27). As a result, it makes the site much broader and shallower as compared with all of the other RIPs. Tyr[241] is the conserved aromatic residue, and Asp[229] and Asn[248] are the polar sugar-binding residues. Only a few polar interactions were observed between the sugar and 2γ-site as compared with the 1α-site. Despite the presence of only a few polar interactions, electron density was exceptionally clear for the complete lactose molecule (Fig. 2C). The galactose ring is oriented parallel to the aromatic ring of Tyr[241] and makes large number of stacking interactions that play a very important role in holding the sugar inside the pocket despite the absence of the supporting kink. The pyranose ring of sugar is rotated at an angle of 180° in comparison to ML-I and ricin, such that the O6 of the galactose bound in ML-I and ricin lies opposite to the O6 of the galactose bound in HmRIP (Fig. 9A). The conserved polar residue Asp[229] Oδ1 interacts with galactose O3 in HmRIP (Fig. 9B). Oδ1 and Oδ2 of the homologous Asp interacts with galactose O4 and O3 in ML-I and ricin and with O3 and O2 in ebulin. The conserved Asn[248] Nδ2 interacts with galactose O3 and O4 in HmRIP and ML-I, but with only O3 in ricin and ebulin. As mentioned earlier, because of the deletion of two residues, the 2γ-site of HmRIP has become much shallower and broader. Therefore, only one interaction is observed between galactose O3 and the main chain carbonyl oxygen of Val[230] from the kink region. As seen in the 1α-site and the 1β-site, sugar makes important interactions with the βI-βII segment. In ricin, galactose O3 interacts with the Nε2 of His[251] belonging to this region. HmRIP, ML-I, and ebulin have a Thr at this site. In ebulin, the sugar has a direct interaction with the Thr because of its deep seated lo-

calization (37); however, in ML-I it is a water-mediated interaction (34). In HmRIP also the interaction is possible through a water molecule, which could not be located because of limitation of the resolution.

HmRIP is known to have equal affinity for galactose and *N*-acetyl galactosamines like ricin (25, 26, 58); however, ML-I has specificity for galactose (59). The affinity of ricin for N-acetyl galactosamine has been associated with its proposed binding through Ser[238] from the kink region; however, the substitution of Ala for Ser in ML-I causes steric hindrance, resulting in its reduced affinity for *N*-acetyl galactosamine (34). The deletion of the corresponding residue in HmRIP has led to the widening of the pocket that provided sufficient space to accommodate the *N*-acetyl group.

As discussed, three structural features have been proposed to date as being essential for a functionally active sugar-binding site (36, 37). A detailed analysis of the active sugar-binding sites of RIPs suggests the importance of another structural feature pertaining to the βI-βII segment connecting the two β-sheets of the subdomain. In the 1α-site, the critical Lys belonging to this region interacts with the sugar. It also stabilizes the conformation of the conserved Asn. In ebulin, although the homologous Lys is mutated to Gly, Gln[44] (numbering of ebulin) from the same segment takes its position and offers the same interactions. In the 2γ-site the homologous region has a His in ricin and Thr in HmRIP, ML-I, and ebulin, which form the interaction with sugar. The 1β-site lacks the conserved polar sugar-binding residues. Instead, the same region moves closer in a way that the main chain nitrogen and oxygen atoms interact with the bound sugar. Thus, the region represents another important structural feature found to be conserved at all the functionally active sugar-binding sites and seems to be important for sugar binding.

The 2γ-site in HmRIP is devoid of a kink region, and the 1β-site lacks the conserved polar sugar-binding residues. Despite these two important features, both of the sites were found
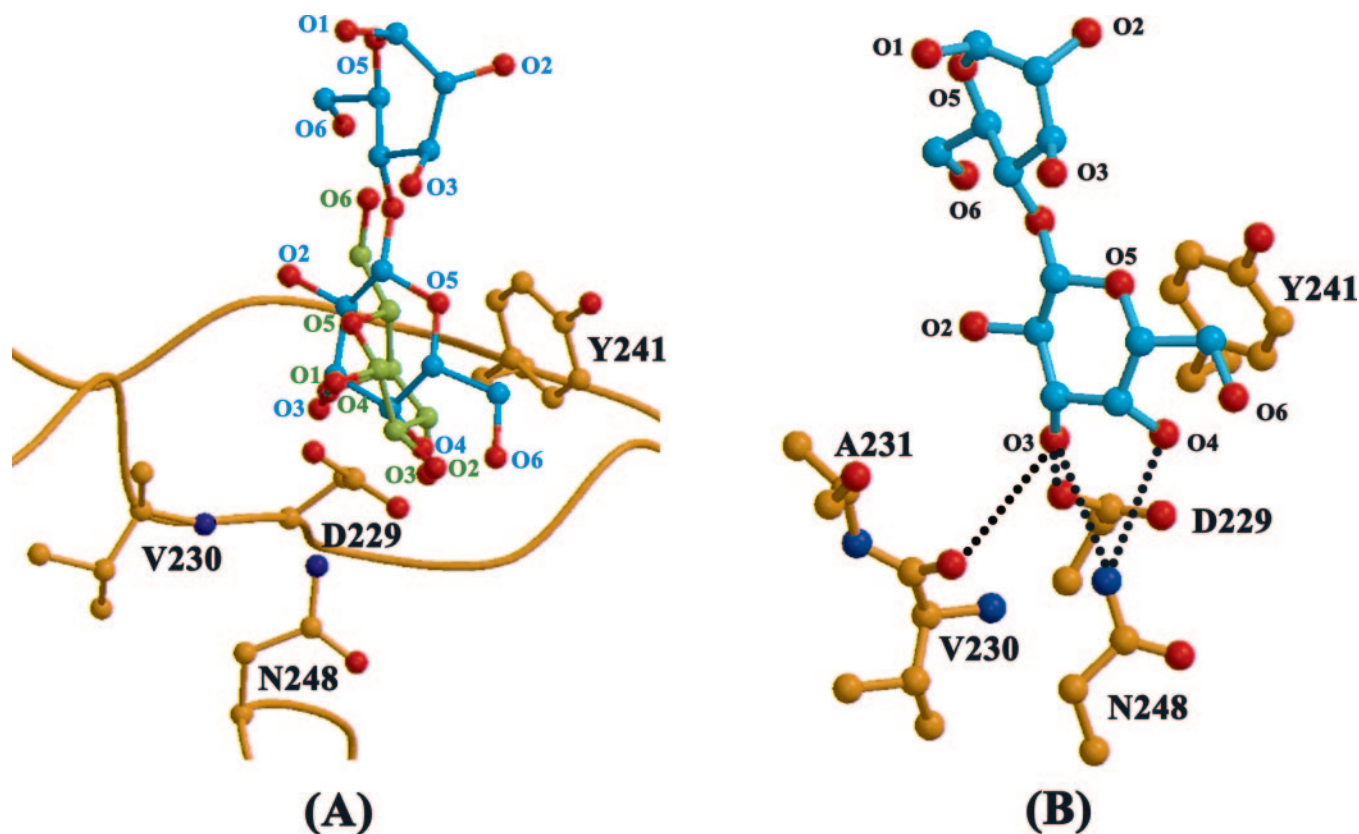
Fig. 9. *A*, superposition of lactose bound at the 2γ sugar-binding site of HmRIP (*cyan*) and ML-I (*green*). The galactose ring is oriented at an angle of 180° in HmRIP as compared with the ML-I, with the O6 of HmRIP and ML-I lying opposite to each other. *B*, interactions between lactose (*cyan*) and sugar-binding residues (*mustard*) at the 2γ-site of HmRIP. Galactose makes stacking interactions with the aromatic ring of Tyr[241] (*Y241*). H-bonds are mainly formed by O3 of the galactose. Single letter amino acid abbreviations are used with position numbers here.

to be functionally active. This indicates that the proposed structural features are important, but not essential, and that a sugar-binding site can be functionally active even if one of these features is missing.

The O3 and O4 hydroxyls of galactose are known to be the most critical moieties for successful saccharide binding in all of the RIPs as well as the galactose-specific lectins (60). The mode of galactose binding in HmRIP reveals that O2 and O3 hydroxyls interact with the conserved Asp, which is the most critical polar residue involved in sugar binding. O2 and O3 are also involved in a number of interactions with other polar residues. O4, on the other hand, does not have any interaction with the conserved Asp. It only has a single nonspecific interaction with a main chain nitrogen atom at the 1α-site and a weak H-bond with the Asn[248] at the 2γ-site. It shows that the hydroxyls mainly involved in the sugar binding in HmRIP are O2 and O3 and not O3 and O4. These results corroborate our earlier observation based on the sugar-binding studies carried out on the HmRIP (25, 61). Although the structure of the HmRIP-lactose complex reveals a unique mode of sugar binding, it does not explain the high affinity of HmRIP for L-rhamnose, L-arabinose, and *meso*-inositol. The molecular basis of the unique sugar affinity of HmRIP can be understood only if more complexes of HmRIP with various sugars are studied structurally.

Conclusion—This is the first time that a natural inhibitor has been detected at the *N*-glycosidase activity site in any type II RIP. This indicates the possible mechanism in plants to prevent cellular autotoxicity because of RIPs. The RIPs seems to get activated only when required to do so, such as upon the attack of plant pathogens. The observation of a bound sugar at the 1β-site has, for the first time, revealed a third functionally

active sugar-binding site in the RIPs. The structure also reveals a novel and versatile mode of sugar binding in HmRIP. These studies have provided the basis for evaluating the binding of different sugars to HmRIP and the design of inhibitors against RIPs.

REFERENCES

1. Nielsen, K., and Boston, R. S. (2001) *Annu. Rev. Plant Physiol. Plant Mol. Biol.* **52,** 785–816
2. Park, S. W., Vepachedu, R., Sharma, N., and Vivanco, J. M. (2004) *Planta* **219,** 1093–1096
3. Park, S. W., Stevens, N. M., and Vivanco, J. M. (2002) *Planta* **216,** 227–234
4. Lam, S. K., and Ng, T. B. (2001) *Arch. Biochem. Biophys.* **393,** 271–280
5. Endo, Y., and Tsurugi, K. (1988) *J. Biol. Chem.* **263,** 8735–8739
6. Peumans, W. J., Hao, Q., and van Damme, E. J. M. (2001) *FASEB J.* **15,** 1493–1506
7. Barbieri, L., Valbonesi, P., Bonora, E., Gorini, P., Bolognesi, A., and Stirpe, F. (1997) *Nucleic Acids Res.* **25,** 518–522
8. Reinbothe, S., Reinbothe, C., Lehmann, J., Becker, W., Apel, K., and Partheir, B. (1994) *Proc. Natl. Acad. Sci. U. S. A.* **91,** 7012–7016
9. Parikh, B. A., and Tumer, N. E. (2004) *Mini Rev. Med. Chem.* **4,** 523–543
10. Bolognesi, A., and Polito, L. (2004) *Mini Rev. Med. Chem.* **4,** 563–583
11. Elhaggar, S. (1993) *Arch AIDS Res.* **7,** 120–121
12. Motto, M., and Lupotto, E. (2004) *Mini Rev. Med. Chem.* **4,** 493–503
13. Harley, S., and Beevers, H. (1982) *Proc. Natl. Acad. Sci. U. S. A.* **79,** 5935–5938
14. Frigerio, L., and Roberts, L. M. (1998) *J. Exp. Bot.* **49,** 1473–1480
15. Elpidina, E. N., Voskoboynikova, N. E., Belozersky, M. A., and Dunaevsky, Y. E. (1991) *Planta* **185,** 46–52
16. Hartley, M. R., Chaddock, J. A., and Bonness, M. S. (1996) *Trends Plant Sci.* **1,** 260–268
17. Desvoyes, B., Poyet, J. C., Schlick, J. L., Adami, P., and Jouvenot, P. D. (1997) *FEBS Lett.* **410,** 303–308
18. Schlick, J. L., Desvoyes, B., Hakil, M., Adami, P., and Dulieu, P. (1999) *Plant Sci.* **140,** 1–10
19. Heiny, B. N., Albrecht, V., and Beuth, J. (1998) *Anticancer Res.* **18,** 583–586
20. Hajto, T., Hostanska, K., and Gabius, H. J. (1989) *Cancer Res.* **49,** 4803–4808
21. Kovacs, E. (2000) *Biomed. Pharmacother.* **54,** 305–310
22. Gabius, H. J., and Gabius, S. (1991) *Lectins and Cancer*, Springer-Verlag, Heidelberg, Germany
23. Lee, R. T., Gabius, H. J., and Lee, Y. C. (1992) *J. Biol. Chem.* **267,** 23722–23727
24. Youle, R. J., Murray, G. L., and Neville, D. M. J. (1981) *Cell* **23,** 551–559

25. Mishra, V., Sharma, R. S., Yadav, S., Babu, C. R., and Singh, T. P. (2004) *Arch. Biochem. Biophys.* **423,** 288–301
26. Otwinowski, Z., and Minor, W. (1997) *Methods Enzymol.* **276,** 307–326
27. Navaza, J. (1994) *Acta Crystallogr. Sect. A* **50,** 157–163
28. Mishra, V., Ethayathulla, A. S., Sharma, R. S., Yadav, S., Krauspenhaar, R., Betzel, C., Babu, C. R., and Singh, T. P. (2004b) *Acta Crystallogr. Sect. D Biol. Crystallogr.* **60,** 2295–2304
29. Murshudov, G. N., Vagin, A. A., Lebedev, A., Wilson, K. S., and Dodson, E. J. (1999) *Acta Crystallogr. Sect. D Biol. Crystallogr.* **55,** 247–255
30. Winn, M. D., Isupov, M. N., and Murshudov, G. N. (2001) *Acta Crystallogr. Sect. D Biol. Crystallogr.* **57,** 122–133
31. Jones, T. A., Zou, J. Y., Cowan, S. W., and Kjeldgaard, M. (1991) *Acta Crystallogr. Sect. A* **47,** 110–119
32. Ramachandran, G. N., and Sasisekharan, V. (1968) *Adv. Protein Chem.* **23,** 283–437
33. Laskowski, R. A., MacArthur, M. W., Moss, D. S., and Thornton, J. M. (1993) *J. Appl. Crystallogr.* **26,** 283–291
34. Niwa, H., Tonevitsky, A. G., Agapov, I. I., Saward, S., Pfüller, U., and Palmer, R. A. (2003) *Eur. J. Biochem.* **270,** 2739–2749
35. Krauspenhaar, R., Eschenburg, S., Perbandt, M., Kornilov, V., Konareva, N., Mikailova, I., Stoeva, S., Wacker, R., Maier, T., Singh, T. P., Mikhailov, A., Voelter, W., and Betzel, C. (1999) *Biochem. Biophys. Res. Commun.* **257,** 418–424
36. Rutenber, E., Katzin, B. J., Ernst, S., Collins, E. J., Mlsna, D., Ready, M. P., and Robertus, J. D. (1991) *Proteins* **10,** 241–250
37. Pascal, J. M., Day, P. J., Monzingo, A. F., Ernst, S. R., Robertus, J. D., Iglesias, R., Perez, Y., Ferreras, J. M., Citores, L., and Girbes, T. (2001) *Proteins* **43,** 319–326
38. Tahirov, T. H., Lu, T. H., Liaw, Y. C., Chen, Y. L., and Lin, J. Y. (1995) *J. Mol. Biol.* **250,** 354–367
39. Gu, Y. J., and Xia, Z. X. (2000) *Proteins* **39,** 37–46
40. Mishra, V. (2004) *Ribosome Inactivating Protein of Viscum album (L.) from North-western Himalaya: Purification and Characterization*. Ph.D. thesis, University of Delhi, Delhi, India
41. Kurinov, I. V., Myers, D. E., Irvin, J. D., and Uckun, F. M. (1999) *Protein Sci.* **8,** 1765–1772
42. Yan, X., Hollis, T., Svinth, M., Day, P., Monzingo, A. F., Milne, G. W. A., and Robertus, J. D. (1997) *J. Mol. Biol.* **266,** 1043–1049
43. Robertus, J. D., Yan, X., Ernst, S., Monzingo, A., Worley, S., Day, P., Hollis, T., and Svinth, M. (1996) *Toxicon* **34,** 1325–1334
44. Oettle, K., and Reibnegger, G. (1999) *Biochim. Biophys. Acta* **1430,** 387–395
45. Bagga, S., Seth, D., and Batra, J. K. (2003) *J. Biol. Chem.* **278,** 4813–4820
46. Ren, J., Wang, Y., Dong, Y., and Stuart, D. (1994) *Structure* **2,** 7–16
47. Ready, M. P., Kim, Y., and Robertus, J. D. (1991) *Proteins* **10,** 270–278
48. Huang, Q., Liu, S., Tang, Y., Jin, S., and Wang, Y. (1995) *Biochem. J.* **309,** 285–298
49. Day, P. J., Ernst, S. R., Frankel, A. E., Monzingo, A. F., Pascal, J. M., Molin-Svinth, M. C., and Robertus, J. D. (1996) *Biochemistry* **35,** 11098–11103
50. Monzingo, A. F., and Robertus, J. D. (1992) *J. Mol. Biol.* **227,** 1136–1145
51. Yan, X., Day, P., Hollis, T., Monzingo, A. F., Shelp, E., Robertus, J. D., Milne, G. W. A., and Wang, S. (1998) *Proteins* **31,** 33–41
52. Rutenber, E., Ready, M., and Robertus, J. D. (1987) *Nature* **326,** 624–626
53. Rutenber, E., and Robertus, J. D. (1991) *Proteins* **10,** 260–269
54. Weis, W. I., and Drickamer, K. (1996) *Annu. Rev. Biochem.* **65,** 441–473
55. Lee, R. T., Gabius, H. J., and Lee, Y. C. (1994) *Carbohydr. Res.* **254,** 269–276
56. Steeves, R. M., Denton, M. E., Barnard, F. C., Henry, A., and Lambert, J. M. (1999) *Biochemistry* **38,** 11677–11685
57. Frankel, A., Tagge, E., Chandler, J., Burbage, C., and Willingham, M. (1996) *Protein Eng.* **9,** 371–379
58. Houston, L., and Dooley, L. (1982) *J. Biol. Chem.* **257,** 4147–4151
59. Ziska, P., Gelbin, M., and Franz, H. (1993) *Lectin Biol. Biochem. Clin. Biochem.* **8,** 10–13
60. Bussing, A. (ed) (2000) *Mistletoe: The Genus Viscum*, Harwood Academic Publisher, Amsterdam
61. Mishra, V., Sharma, R. S., Paramasivam, M., Bilgrami, S., Yadav, S., Srinivasan, A., Betzel, C., Babu, C. R., and Singh, T. P. (2005) *Plant Sci.* **168,** 615–625
62. Esnouf, R. M. (1997) *J. Mol. Graph. Model* **15,** 132–134
63. Kraulis, P. J. (1991) *J. Appl. Crystallogr.* **24,** 946–950
64. Merritt, E. A., and Murphy, M. E. P. (1994) *Acta Crystallogr. Sect. D Biol. Crystallogr.* **50,** 869–873